# Speed Ripple Minimization of Permanent Magnet Synchronous Motor Based on Model Predictive and Iterative Learning Controls

**QIANG FEI[1,2], YONGTING DENG[1], (Member, IEEE), HONGWEN LI[1], (Member, IEEE), JING LIU[1], (Member, IEEE), AND MENG SHAO[1,2]**
[1]Changchun Institute of Optics, Fine Mechanics and Physics, Chinese Academy of Sciences, Changchun 130033, China
[2]University of Chinese Academy of Sciences, Beijing 100049, China

Corresponding author: Yongting Deng (dyt0612@163.com)

**ABSTRACT** Permanent magnet synchronous motors (PMSMs) are widely used in the field of industrial servo control, especially in high-precision applications. Owing to the periodic torque ripple caused by the cogging torque, flux harmonics, and current offsets, the speed output of the system has a periodic ripple, which affects the control accuracy of the servo system. The conventional proportional–integral controllers cannot reject torque ripple and are highly dependent on motor parameters. This limits the control performance when a PMSM is used as a high-precision servo system. Thus, this paper proposes a combination of model predictive control (MPC) and iterative learning control (ILC) to not only speed up the response time of the system but also effectively reduce the speed ripples. MPC updates the predictive model in real time through feedback and evaluates the system output and control rate according to the cost function. It obtains an optimal control sequence for the next moment and has good parameter robustness and fast response. ILC records the speed of ripple signals over an entire cycle and then uses those signals to compensate for the control signal in the next cycle. It is capable of reducing the periodic speed ripples. The experimental verification of the schemes was conducted on a digital signal processor–field programmable gate-array-based platform. The experimental results obtained confirm the effectiveness of the proposed MPC–ILC scheme.

**INDEX TERMS** Iterative learning control, model predictive control, PMSM control, speed ripple.

## I. INTRODUCTION

A permanent magnet synchronous motor (PMSM) is widely used in the field of industrial servo control, especially in high-precision fields such as robotics, aerospace, and large telescopes. PMSMs are preferred over dc motor drives, which are conventionally used for ac servo drives, mainly because of their advantages such as high power density, high torque-to-inertia ratio, and high efficiency [1].

However, the parasitic torque ripples in PMSM are inevitable, and their effect on motion control and precision in applications is undesirable. These torque ripples lead to periodic speed oscillations, which cause degradation in the drive performance, especially in low-speed operations [2]. If the

The associate editor coordinating the review of this manuscript and approving it for publication was Fangfei Li.

velocity fluctuates too much, it may even cause instability in the servo system.

Torque pulsations in a PMSM are caused by various sources, such as cogging, flux harmonics, errors in current measurements, and phase unbalancing [3]. In addition, the time delay due to data processing in the microprocessor must be considered [4]. Many techniques have been proposed in the past two decades to minimize torque ripples and can be broadly classified into two categories [5].

The first category involves the design and improvement of the motor body structure, such as skewing the slot or magnet, ensuring a fractional number of slots per pole, and improving the winding distribution [6], [7]. Although improving the motor structure is the most effective and reliable method, such methods are not repeatable. In other words, once the designed motor is produced, the motor performance cannot

be modified. Moreover, the special machine-design processes require complex production processes, resulting in a higher machine cost. The second approach involves the use of active control schemes. Many scholars have proposed control algorithms to improve the performance of motors by designing a controller to correct and compensate the periodic torque ripple.

The second method was the main research direction of the current study. The focus was on using additional control measures to compensate for these periodic torque ripples. Many composite methods are proposed by researchers to deal with the torque ripple and simultaneously improve the performance robustness of the control system [8], [9].

As an advanced control strategy, predictive control has been studied by many scholars and achieved satisfactory results. Model predictive control (MPC) is considered by many researchers to be one of the most robust control techniques and a possible candidate for electrical drives. MPC is based on the optimization of the cost function, which is related to the difference between the output and desired trajectory [6]. MPC comprises three steps: predictive model, receding optimization, and feedforward–feedback structure. The MPC method has advantages such as robustness, simple modeling, and ability to handle control variable constraints; these can ensure satisfactory performance of the system [10].

In recent years, with the development of faster microcontrollers and advances in MPC research, a number of compound algorithms based on MPC have been proposed to reduce the torque ripple and enhance the control performance of PMSMs [11]–[21]. To compensate for the torque ripple caused by cogging, a hybrid method that uses the FCS-MPC and a look-up table was presented to obtain good cogging-torque estimation [11]. Other improvements, such as quantitative search [12] and duty cycle control [13], [14] have also been proposed. Several of the above modifications can reduce torque and current ripples. In addition, some scholars have proposed a control strategy combining MPC with observers [15]–[18]. The estimated disturbance is used to compensate for the uncertainties of the current or speed loop through a feed-forward control. In [17], a continuous-time model predictive control (CTMPC) for a PMSM drive was discussed; the CTMPC uses a Taylor series expansion to derive a closed-form solution to the MPC problem, and a nonlinear disturbance observer was designed to enhance the prediction accuracy under parameter variation and unknown load torques. These experiments showed that this method showed good transient and steady-state performances. However, this approach can be used only for torque ripple components that are observable from an electrical subsystem; ripples due to a mechanical part (e.g., cogging torque and load oscillations) cannot be observed or controlled [19]. In [20], a cascade MPC structure was proposed for a PMSM with current and speed control as the inner and outer loops, respectively. To reduce the impact of periodic disturbances arising from the offset errors of the current sensor on the speed control of a PMSM, a disturbance model, with the signal

generators of zero and first frequency modes, was embedded in the design of the outer-loop MPC. However, the established torque-ripple model is often complicated and inaccurate [21], and provides limited suppression of torque ripple.

In the PMSM control system, the occurrence of torque ripple is mainly related to the rotor position, which causes periodical oscillations of the machine torque and speed. Iterative learning control (ILC) is widely used as a model-free control strategy to suppress periodic torque ripple. ILC is an approach to improve the performance of a system that is executed repetitively and periodically over a fixed time interval by learning from previous executions (trials, iterations, and passes) [22]. ILC has significant control effects on the abovementioned repetitive problems [23]–[25]. In [23], a modified ILC scheme was implemented in the frequency domain via a Fourier series expansion is presented, combined with the PI speed controller to further suppress torque ripple. Combining ILC with second-order sliding mode technology suppresses torque ripple and is also robust to noise [25]. As possible sources of torque ripple are observable based on the rotor speed, ILC is often utilized in combination with a speed controller in the speed loop.

This paper presents an MPC–ILC scheme, which uses the dynamic discrete system in the PMSM to design a predictive model with periodic perturbation and uses the angle-based ILC to learn and store the velocity error to compensate the velocity loop control in the next cycle. ILC is used to suppress the speed ripple caused by the torque ripple, while MPC improves the response speed and robustness of the system. The performance of the MPC-ILC scheme was verified through multiple experiments. The experimental results show that the proposed method shows significant improvements in terms of speed ripple reduction and response speed.

The remainder of this paper is organized as follows. Section II introduces the mathematical model of the PMSM. Section III discusses the source of torque ripples due to cogging, flux harmonics, current offsets, and scaling errors. Further, Section IV presents the design process of the MPC combined with ILC based on a discredited model of the PMSM. The implementation, simulation, and experiment are discussed in Section V, and Section VI presents the experimental results and discussion. Finally, the paper is concluded in Section VII.

## II. MATHEMATICAL MODEL OF PMSM

To analyze the variable speed drive system of a PMSM, the motor must be modeled properly. First, the following assumptions were made about the PMSM used in this study.

1) The neutral point is not connected.
2) Iron saturation is negligible.
3) There are no eddy currents or core losses. In other words, the magnetic permeability of the core is infinite, and the eddy-current and hysteresis losses of stator and rotor cores are ignored.
4) The motor parameters (winding resistance and winding inductance, etc.) are constant.

Based on these assumptions, the stator $d$–$q$ axis voltage equations of the PMSM in the synchronous rotating reference frame can be expressed as follows:

$$\frac{di_d}{dt} = \frac{1}{L_d}(u_d - R_s i_d + \omega_e L_q i_q) \tag{1}$$

$$\frac{di_q}{dt} = \frac{1}{L_q}(u_q - R_s i_q - \omega_e L_d i_d - \omega_e \psi_f) \tag{2}$$

$$\frac{d\omega_e}{dt} = \frac{1}{J}(T_e - B\omega_e - T_L) \tag{3}$$

$$T_e = \frac{3}{2}p[\psi_f i_q + (L_d - L_q)i_d i_q] \tag{4}$$

Here, $i_d$ and $i_q$ are the stator currents along the $d$ and $q$ axes, respectively; $u_d$ and $u_q$ denote the stator voltage in the $d$–$q$ frame; $R_s$ is the stator resistance; $\omega_e$ is the electrical angular speed. Here, $\omega_e = p\omega_m$, where $\omega_m$ denotes the mechanical speed and $p$ is the number of pole pairs. Furthermore, $\psi_f$ is the PM flux linkage, $T_L$ is the load torque, and $J$ and $B$ are the moment of inertia and viscous coefficient of load, respectively.

As the surface-mounted PMSM is nonsalient, the $d$-axis inductance is equal to that of the $q$ axis, i.e., $L_d = L_q = L$. Hence, a reluctance torque component does not exist. The motor torque coefficient is $K_t = 3p\psi_f/2$.

By using a usual field-oriented control of the PMSM, the stator current was controlled to obtain a right angle between the stator current and rotor flux ($i_d = 0$), and therefore did not contribute toward magnetization but only toward torque production, and (4) is re-expressed as

$$T_e = K_t i_q. \tag{5}$$

By substituting (5) into (3), the mechanical dynamic is described as follows:

$$J\frac{d\omega_e}{dt} = K_t i_q - B\omega_e - T_L. \tag{6}$$

## III. ANALYSIS OF TORQUE RIPPLES
The torque ripple of the PMSM is mainly divided into two types. The first type is the torque ripple caused by the motor body structure, e.g., the cogging torque and flux harmonics, whereas the second type is caused by the drive controller, e.g., the current measurement error, data processing delay, and dead time effect. The generation principle of a torque ripple is the interaction between the stator current and rotor magnetic field. The parasitic torque ripple in a PMSM will cause the cyclical fluctuation of the electromagnetic torque, which will cause speed fluctuation in the steady state and affect the control precision of the motor.

The cogging torque was analyzed from the structure of the motor. From the perspective of energy, the energy storage in the air gap of the stator slot was not constant, and the fluctuation in this energy caused the torque fluctuation. According to mechanical analysis, the torque is caused by the interaction between the magnetic flux and stator slots, and the permanent magnet is subjected to a tangential force, which moves toward the direction of the stator tooth.

The compensation of this problem using a mathematical method is very difficult because of the lack of a precise cogging torque model. According to the analysis presented in [26], the cogging torque can be simplified as a periodic function of the rotor position, and can be represented by a Fourier series [27].

$$T_{cogg}(\theta_m) = \sum_{k=1}^{\infty} T_{mk} \sin(mk\theta_m), \tag{7}$$

where $\theta_m = \theta_e/p$ is the angular position, $T_{mk}$ represents the Fourier coefficients, and $m$ is the least common multiple of stator slots $Ns$ and the number of poles $2p$.

Magnetic flux harmonics are also an important cause of torque pulsation. Owing to the motor structure and defect of motor processing, the air-gap magnetic density of the motor is nonsinusoidal; for example, the existence of the motor slot structure can destroy the sinusoidal nature of the flux density. This results in an imperfect sinusoidal flux-density distribution that produces periodic torque ripple when interacting with standard stator currents. In the $d$–$q$ frame, the flux harmonics appear as the sixth, twelfth, and other multiples of the sixth harmonics, and can be expressed as

$$\psi_d(\theta_e) = \psi_{d0} + \psi_{d6}\cos(6\theta_e) + \psi_{d12}\cos(12\theta_e) + \cdots, \tag{8}$$

where $\psi_{d0}$ is the fundamental component; $\psi_{d6}$ and $\psi_{d12}$ are the sixth and twelfth harmonic terms of the $q$-axis flux linkage, respectively; $\theta_e$ is the electrical angle. The combination of (5) and (8) yields

$$T_m = T_0 + T_6\cos(6\theta_e) + T_{12}\cos(12\theta_e) + \cdots, \tag{9}$$

where $T_0$ is the fundamental component, and $T_6$ and $T_{12}$ are the 6th and 12th harmonic torque amplitudes, respectively. Equation (9) indicates that the 6th and 12th torque harmonics produced mainly owing to the nonsinusoidal flux distribution are periodic in nature. Therefore, the harmonic torque can also be considered as a function of the mechanical angle.

Current offsets and scaling errors belong to the inevitable situation caused by the controller. During measurement, inaccurate current acquisition introduces measurement noise, causing a DC offset. The output of the current sensor must be scaled to match the input of the A/D converter, and in the digital form, the controller rescales the value of the A/D output to obtain the actual value of the current, thus introducing a scaling error.

In [3], the torque ripple caused by the current offset error is expressed as

$$\Delta T_{offset} = K_t \frac{2}{\sqrt{3}}\cos(\theta_e + \alpha)\sqrt{\Delta i_{as}^2 + \Delta i_{as}\Delta i_{bs} + \Delta i_{bs}^2}, \tag{10}$$

where $\Delta a$ and $\Delta b$ are the DC offsets in the measured currents of phases $a$ and $b$, respectively, $\theta_e = 2\pi f_s t$, and $\alpha$ is the constant angular displacement and is dependent on phase currents. In addition, the scaling factors for the currents of phases $a$ and $b$ are denoted as $K_a$ and $K_b$, respectively.

The torque ripple caused by the current scaling error is expressed as

$$\Delta T_{scaling} = K_t(\frac{K_a - K_b}{K_a K_b})\frac{I}{\sqrt{3}}\left[\cos(2\theta_e + \frac{\pi}{3}) + \frac{1}{2}\right], \quad (11)$$

Equations (10) and (11) show that the DC offset in the current measurement causes a torque oscillation at the fundamental frequency and the scaling error causes the torque to oscillate at twice the fundamental frequency.

## IV. DESIGN OF THE PROPOSED CONTROLLER

As the main controller of the speed loop, the MPC updates a state by receding the time domain strategy and processes the parameter perturbation caused by various uncertain disturbances and operating environments online to improve the robustness of the system. The MPC translates PMSM control issues into output optimization issues. The prediction and optimization are based on the real-time feedback information of the system, and the initial value of each prediction model is updated. Therefore, MPC does not need a high-precision PMSM model and can achieve a better control effect.

Fig. 1 shows the block diagram of the MPC, the purpose of which is to accurately track the reference speed. The control value is obtained by minimizing the value function after multistep prediction.
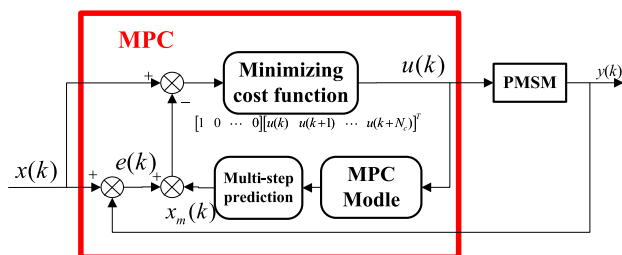


**FIGURE 1.** MPC diagram.

### A. DESIGN MODEL FOR THE OUTER-LOOP MPC

According to (6), the PMSM model is described as follows, considering the periodic disturbances:

$$J\frac{d\omega}{dt} = K_t i_q - B\omega + f(\omega, t), \quad (12)$$

where $f(\omega, t)$ is an unknown periodic function resulting from torque ripple. The MPC requires a discrete model of the PMSM, thus requiring the use of Euler discretion, and $T_s$ is sample period. The discrete mechanical equations can be obtained as follows:

$$\omega(k + 1) = (1 - \frac{BT_s}{J})\omega(k) + \frac{K_t T_s}{J}i_q(k) + \frac{T_s}{J}f(\omega, k). \quad (13)$$

Then, by defining state variable $x(k) = \omega(k)$, $u(k) = i_q(k)$, $A_m = (1 - \frac{BT_S}{J})$, $B_m = \frac{K_t T_s}{J}$, and $C_m = \frac{T_s}{J}$, (13) can be rewritten as

$$x(k + 1) = A_m x(k) + B_m u(k) + C_m f(x, k). \quad (14)$$

Upon formulation of the mathematical model, the next step in the design of a predictive control system is to calculate the predicted plant output by using the future control signal as the adjustable variable. The predicted state can be expressed as

$$\begin{aligned} x(k+2|k) &= A_m x(k+1|k) + B_m u(k + 1) + C_m f(x, k + 1) \\ &= A_m^2 x(k) + A_m B_m u(k) + B u(k + 1) \\ &\quad + A_m C_m f(\omega, k) + C_m f(\omega, k + 1) \quad (15) \end{aligned}$$

$$\begin{aligned} x(k+N_p|k) &= A_m x(k + N_p - 1|k) + B_m u(k + N_p - 1) \\ &\quad + C_m f(x, k + N_p - 1) \\ &= A_m^{N_p} x(k) + A_m^{N_p - 1} B_m u(k) \\ &\quad + \cdots + (A_m^{N_p - N_c} B_m + \cdots + B_m) u(k + N_c - 1) \\ &\quad + A_m^{N_p - 1} C_m f(\omega, k) + \cdots + C_m f(\omega, k + N_p) \end{aligned}$$

$$(16)$$

where $N_p$ and $N_c$ are the prediction and control horizons, respectively. Control horizon $N_c$ was selected as less than (or equal to) prediction horizon $N_p$. The term $x(k + N_p|k)$ is the $N_p$ th step predicted state variable at the $k$th moment, and the vectors are defined as

$$X(k) = [x(k + 1|k), x(k + 2|k), \cdots, x(k + N_p|k)]^T$$
$$U(k) = [u(k), u(k + 1), u(k + 2), \cdots, u(k + N_c - 1)]^T$$
$$F(k) = [f(k), f(k + 1), f(k + 2), \cdots, f(k + N_p - 1)]^T$$

The matrix form of the predicted state variable can be expressed as

$$X = Gx(k) + \Phi U + \varepsilon F, \quad (17)$$

where

$$G = \begin{bmatrix} A_m \\ A_m^2 \\ A_m^3 \\ \vdots \\ A_m^{N_p} \end{bmatrix} \quad \varepsilon = \begin{bmatrix} A_m^{N_p - 1} C_m \\ A_m^{N_p - 2} C_m \\ \vdots \\ A_m C_m \\ C_m \end{bmatrix}^T$$

$$\Phi = \begin{bmatrix} B_m & 0 & 0 \\ \vdots & \vdots & 0 \\ A_m^{N_c - 1} B_m & \cdots & B_m \\ \vdots & & \vdots \\ A_m^{N_p - 1} B_m & \cdots & \sum_{i=0}^{N_p - N_c} A_m^i B_m \end{bmatrix}$$

The main goal of the MPC is to ensure the speed can follow the reference speed accurately, where we assume that the reference speed remains constant in the prediction horizon. For the speed-loop MPC system, the control objective is to find optimal control input $U$ that minimizes the cost function:

$$J = \|W - X\|_Q^2 + \|U\|_R^2, \quad (18)$$

where $Q$ and $R$ are the appropriate dimensions of the output and control weighting matrices, respectively, and positive definite (denoted as $> 0$) $W = \begin{bmatrix} \omega_r(k + 1) & \omega_r(k + 2) & \cdots \end{bmatrix}$

$\omega_r(k + N_p)]^T$ is a vector representation of the output expectation. By substituting (17) into (18), and according to the first derivative of cost function $J$,

$$\frac{\partial J}{\partial U} = -2\Phi^T(W - Gx(k) + \varepsilon F) + 2(\Phi^T\Phi + R)U. \quad (19)$$

Let $\frac{\partial J}{\partial U} = 0$, then optimal control $U$ at the $k$th instant can be obtained as

$$U = (\Phi^T Q\Phi + R)^{-1}\Phi^T Q[W - Gx(k) + \varepsilon F]. \quad (20)$$

However, $F$ is an unknown periodic perturbation sequence; thus, assume that $\hat{F}$ is an estimated sequence of $F$ and is introduced to compensate for unknown periodic disturbances and improve the system's anti-disturbance capability. The next section details an integrated feed-forward compensation design method with the ILC.

Using the terminal constraints and Lyapunov stability theorem to prove the stability of the proposed method. according to (14), the discrete state equation of the system is written as

$$x(k + 1) = g(x(k), u(k)), \quad (21)$$

where $g(\cdot)$ is a nonlinear function, $g(\mathbf{0}, \mathbf{0}) = \mathbf{0}$ is the system input, and the state constraints are $x \in \Omega_x$, $u \in \Omega_u$, $\mathbf{0} \in \Omega_x$, and $\mathbf{0} \in \Omega_u$. By minimizing the cost function (18), the following formula was obtained:

$$\min_{u(k+i|k),0\leq i\leq N-1} J_N(k) = \sum_{i=0}^{N-1} l(x(k + i|k), u(k + i|k))$$

$$s.t.\ x(k + i + 1|k) = g(x(k + i|k), u(k + i|k)),$$

$$i = 0, \cdots, N$$

$$- 1x(k + i|k) \in \Omega_x u(k + i|k) \in \Omega_u$$

$$x(k|k) = x(k) \quad (22)$$

where $l$ is a nonlinear performance function, and $l(\cdot, \cdot) \geq 0$ only if $l(\mathbf{0}, \mathbf{0}) = 0$. Additionally, the terminal constraint $x(k + N|k) = 0$. Assuming that the optimal solution at time k is $U^*(k) = \{u^*(k|k), \cdots, u^*(k+N-1|k)\}$, the corresponding system status is $X^*(k) = \{x^*(k+1|k), \cdots, x^*(k+N|k)\}$, and the optimal value of the performance index can be obtained.

$$J_N^*(k) = \sum_{i=0}^{N-1} l(x^*(k + i|k), u^*(k + i|k)) \quad (23)$$

At time k + 1, a solution $U(k + 1) = \{u(k + 1|k + 1), \cdots, u(k + N - 1|k + 1), 0\}$ was constructed, where $u(k + i|k + 1) = u^*(k + i|k), i = 1, \cdots, N - 1$. The system state is $X(k + 1) = \{x(k + 2|k + 1), \cdots, x(k + N + 1|k + 1)\}$ according to the solution for time k+1, and $x(k+i+1|k+1) = x^*(k + i + 1|k), i = 1, \cdots, N - 1$. Thus, we obtained

$$x(k + N + 1|k + 1) = g(x(k + N|k + 1), u(k + N|k + 1))$$

$$= g(x^*(k + N|k), 0)$$

$$= 0 \quad (24)$$

This shows that $U(k + 1)$ and $X(k + 1)$ meet all the constraints of (22). $U(k+1)$ is a feasible solution. Therefore,

$$J_N^*(k + 1) \leq J_N(k + 1).$$

Further, the optimized performance index value corresponding to $U(k + 1)$ is as follows:

$$J_N(k + 1) = \sum_{i=0}^{N-1} l(x(k + i + 1|k + 1), u(k + i + 1|k + 1))$$

$$= \sum_{i=0}^{N-2} l(x^*(k + i + 1|k), u^*(k + i + 1|k))$$

$$+ l(x(k + N|k + 1), u(k + N|k + 1))$$

$$= J_N^*(k) - l(x^*(k|k), u^*(k|k)) \leq J_N^*(k)$$

This shows that

$$J_N^*(k + 1) \leq J_N^*(k). \quad (25)$$

The equal sign is valid only if $x(k) = 0$ and $u^*(k|k) = 0$. Therefore, using $J_N^*(k)$ as a Lyapunov function, we could prove that the predictive control system was stable.

## B. DESIGN OF ILC TO COMPENSATE FOR PERIODIC DISTURBANCES

ILC is a model-free control method based on a memory mechanism that can cause the error signal to tend to zero in a limited time through the continuous learning of periodic error signals. By considering the above-mentioned analysis of torque ripple, PMSM with periodic torque ripple can be considered as a process with a periodic disturbance. As an iterative method, ILC has a good performance when rejecting a periodic disturbance. Compared to other kinds of active control methods, ILC has the following advantages. It changes the control signal, implying that the structure of the previous control system does not need to be changed, and it is insensitive to plant parameter variations. Therefore, the use of ILC to achieve torque ripple reduction is reasonable.

For the conventional time-based ILC algorithm, the PMSM dynamic system is described as

$$\dot{x}(t) = ax(t) + bu(t) + f(x, t), \quad (26)$$

where $a = -B/J$ and $b = K_t/J$. $f(x, t)$ is a periodic disturbance. In the classic P-type ILC control, the control rate is expressed as

$$u_{i+1}(t) = u_i(t) + \Phi e_i(t), \quad (27)$$

where $i$ indicates the current iteration index, $u_i(t)$ is the control signal generated from the ILC, $e_i(t) = \omega^{ref} - \omega^m$ is the error signal at the $k$th iteration, $\omega^{ref}$ is the reference output, $\omega^m$ is the measured output, and $\Phi$ is the learning gain.

For convergence of the ILC system, given as the learning gain, the following criterion must hold [3]:

$$\|I - b\Phi\| < 1. \quad (28)$$

However, time-based ILC has the following disadvantages for PMSM torque-ripple compensation. The iteration period of time-based ILC must be an integer multiple of the torque-ripple period because torque ripple is a function of angular position, which requires the accurate measurement of the constant velocity value and calculation of the pulsation period,

and then compensate for the disturbance at the corresponding angular position at time $k$. If the speed value changes, the corresponding period must be recalculated. In the case of high control accuracy, once the corresponding angular position is deviated, the system performance may be deteriorated.

In this paper, an angle-based ILC algorithm is proposed. According to the angular position information, the torque ripple is compensated to improve the performance of the system against periodic disturbances. The control algorithm is as follows:

$$\hat{F}_{i+1}(\theta_{m,k}) = (1 - \alpha)\hat{F}_i(\theta_{m,k}) + \Phi e_i(\theta_{m,k}) + \Gamma e_{i+1}(\theta_{m,k}), \quad (29)$$

where $\alpha$ is a forgetting factor to increase the robustness of the algorithm against noise, $\Phi$ is the previous cycle error feedback gain, $\Gamma$ is the current cycle error feedback gain, and $\theta_{m,k}$ indicates the angle value at time $k$.

Then, the conditions for convergence can be obtained according to (28).

$$\left\| 1 - \frac{K_t}{J}\Phi \right\| < 1 \quad (30)$$

As long as $\Phi$ satisfies the above inequality, iterative learning control can achieve stability and convergence. According to [28], $\Gamma$ does not affect the convergence of the learning controller; however, experiments have proved that if $\Gamma$ is extremely large, which would cause the current cycle error and noise to be over-amplified, thus causing the corresponding control output to be larger, eventually leading to the nonconvergence of the system.

### C. OVERALL CONTROL STRUCTURE

Fig. 2 shows the overall structural diagram of the PMSM servo system, that is, the combination of MPC and angle-based ILC to solve the problem of torque ripple minimization. Current decoupling was performed using vector control to transform the three-phase ac currents $i_a$, $i_b$, and $i_c$ into their representations $i_d$ and $i_q$, respectively. The current loop uses the PI controller to track output $i_q$ of the speed loop to generate the control voltage. To suppress the high-frequency noise in the speed signal, the low-pass filter was used.
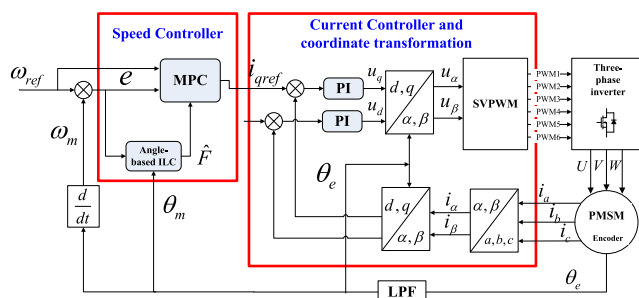
## V. IMPLEMENTATION AND SIMULATION

The system was simulated using MATLAB software tools to demonstrate the effectiveness of the proposed control method, and simulation comparison was conducted between a conventional PI-ILC and the proposed algorithm. For comparison purposes, the current loops of both methods use a PI controller with the same parameters. The PMSM specification and parameters for the simulation are presented in Table 1.

**TABLE 1.** Parameters of PMSM.

| Symbol | Description | Value |
|--------|-------------|-------|
| $P$ | Rated power | 5 KW |
| $T$ | Rated torque | 1606 Nm |
| $R$ | Armature resistance | 2.44 $\Omega$ |
| $L$ | Armature inductance | 36.05 mH |
| $Kt$ | Torque constant | 142.2 Nm/A |
| $p$ | Number of pole pairs | 65 |
| $J$ | Inertia | 3.40 kg.m$^2$ |

The important parameter of the cost function is length $N_p$. Considering the actual application, a very long length of the prediction horizon will increase the computational burden of the processor; however, a lower bound of the length also exists. In other words, input signal $u$ at time step $k$ will affect the voltage, current $i$, and speed $\omega_m$ at time steps $k + 1$, $k + 2$, and $k + 3$, respectively. This sets a minimum value $N_p = 4$ for the prediction horizon. In this study, this value was taken as $N_p = 5$. To shorten the calculation time, the authors considered $N_c = 1$. The parameters of the current PI controllers in the two methods are all the same, that is, for the $q$-axis controller, $K_{ip} = 8$ and $K_{ii} = 0.01$; for the $d$-axis controller, $K_{ip} = 8$ and $K_{ii} = 0.01$; and for the PI speed controller, $K_{sp} = 0.05$, $K_{si} = 0.007$. and. The parameters of the proposed speed controller are $N_p = 5$, $N_c = 1$. Weighting matrices $Q = 1.1 \times I_{5 \times 5}$ and $R = 1$, and the $\alpha = 0.1$, $\Phi = 0.5$, $\Gamma = 0.01$.

Fig. 3 shows the comparison between different strategies. To test the speed response, a speed command from 0 to $5°\,\text{s}^{-1}$ is applied to the speed controller. As shown, the speed response time of the MPC is approximately 0.015 s, which is significantly faster than the PI control strategy, and the overshoot is smaller.
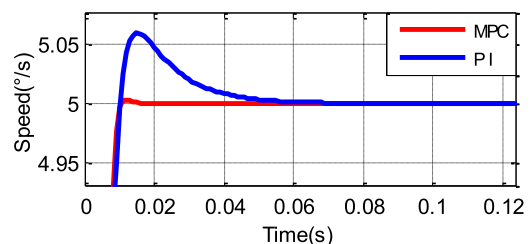


**FIGURE 2.** Overall structural diagram of the PMSM servo system.



**FIGURE 3.** Simulation results of the motor response waveforms of the MPC and PI.
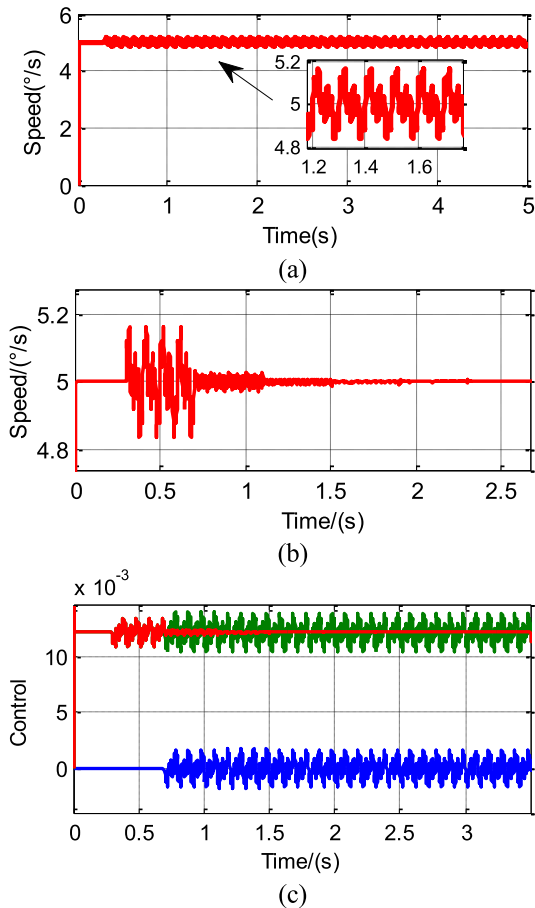
**FIGURE 4.** Simulation results of the velocity pulsation suppression process at 5° s⁻¹.



**FIGURE 5.** Telescope PMSM servo platform.



**FIGURE 6.** Experimental results of speed response at 5° s⁻¹: (a) speed response, (b) Q axis current, and (c) velocity pulsation suppression.

Fig. 4 shows the comparison results of the simulations conducted using the MPC strategy without and with the compensation from ILC at the speed reference of 5° $s^{-1}$. At $t = 0.3$ s, the first, second, and sixth disturbances were added into the speed signal. Fig. 4(a) shows that the MPC has a poor suppression effect on periodic pulsation, whereas Fig. 4(b) shows that when the compensation from ILC is added into the MPC at $t = 0.3$ s, the periodic pulsation is well suppressed after four cycles of iterative learning. In Fig. 4(c), the blue curve represents the control sequence of the ILC to compensate for periodic disturbances, the red curve indicates MPC control, and the green one indicates composite control.

## VI. EXPERIMENTAL RESULTS AND ANALYSIS

To verify the practicability and validity of MPC with ILC, the control algorithms were implemented in a digital signal processing/field programmable gate array (DSP-FPGA)-based azimuth axis platform of a telescope (Fig. 5). The stability of the servo platform of the telescope affects the quality of target imaging, and thus studying the suppression of torque ripple is extremely significant. In the control driver, the FPGA is mainly used for AD conversion, encoder reading, speed detection, and generation of IGBT gate-switching signals.
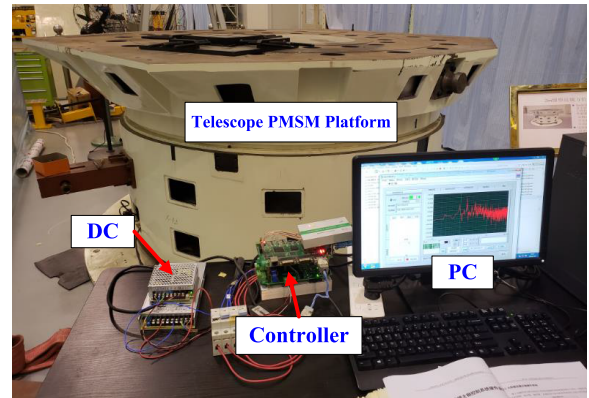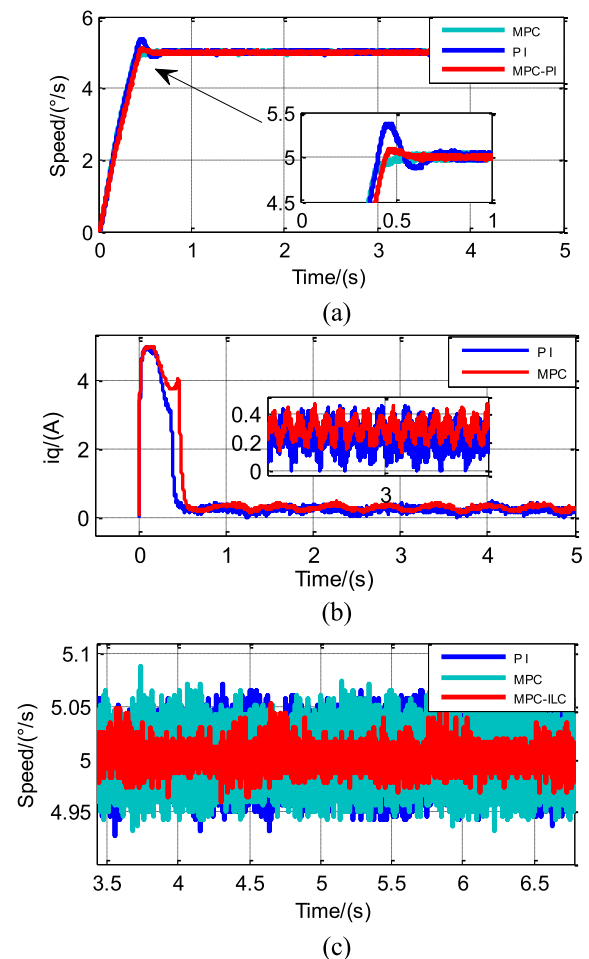
The proposed algorithm was implemented using a C-program in DSP-TMS320F28335. The sampling frequencies for the speed and current controllers were 1 and 15 kHz, respectively. Table 1 lists the parameters of the motor.

During the transient state, the ILC is turned off and $i_{qref}$ is provided only by the MPC controller output. When the
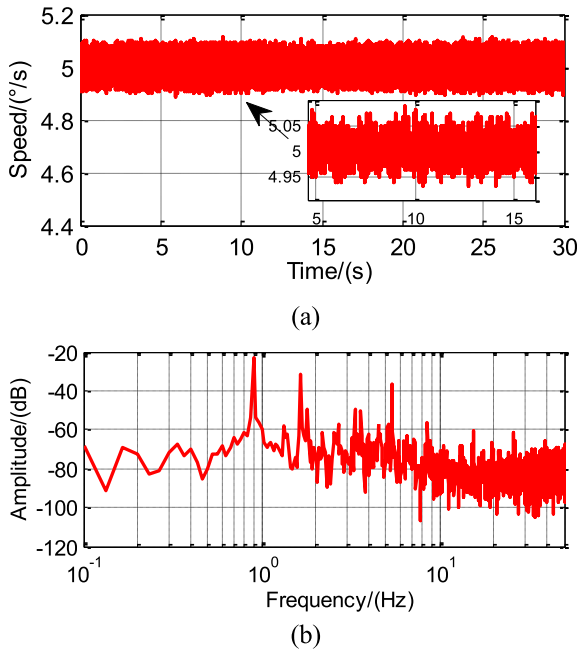
**FIGURE 7.** Experimental results of the PI control at 5° s⁻¹: (a) speed response and (b) frequency spectrum.



**FIGURE 8.** Experimental results of the MPC–ILC control at 5° s⁻¹: (a) speed response and (b) frequency spectrum.



**FIGURE 9.** Experimental results of the PI control at 10° s⁻¹: (a) speed response and (b) frequency spectrum.

steady state is reached, the ILC learns the periodic torque ripple through iteration and compensates for it in the MPC controller to generate the desired current control signal.

The performance of the drive system using the proposed control scheme was compared to the classic PI controller solution. The ratio of the peak-to-peak speed to the average speed was used to evaluate the effectiveness of the proposed scheme for minimizing the torque pulsation, i.e., $SRF = S_{pp}/S_{ave}$.

Based on the theoretical analysis and experimental-platform construction discussed above, experimental results were obtained and are shown in Figs. 6–10. To verify the effectiveness of the proposed algorithm, the experiments were conducted under operating conditions with different speeds: motor speed at 5 and 10° s⁻¹. Fig. 6 shows the velocity response curves corresponding to the PI control, MPC control, and MPC–ILC algorithm at 5° s⁻¹, the corresponding current response result, and the ability to suppress velocity pulsations. Figs. 7–10 show the results of the speed fluctuations of the conventional PI, proposed algorithm, and the Fourier analysis of the corresponding speed. According to the torque analysis presented in Section III, we selected only the first, second, and sixth harmonics for analysis.

The experimental results show that the proposed control algorithm has faster speed response and pulsation suppression capability compared to conventional PI control. In Fig. 6, the MPC–ILC speed response time is 0.6 s, which is 0.2 s faster than the PI control, and the step response shows almost no overshoot. In Fig. 6(b), the Q-axis current fluctuation of the proposed algorithm is slightly smaller than that of the conventional PI. Figs. 7(a) and 8(a) show the speed signals of
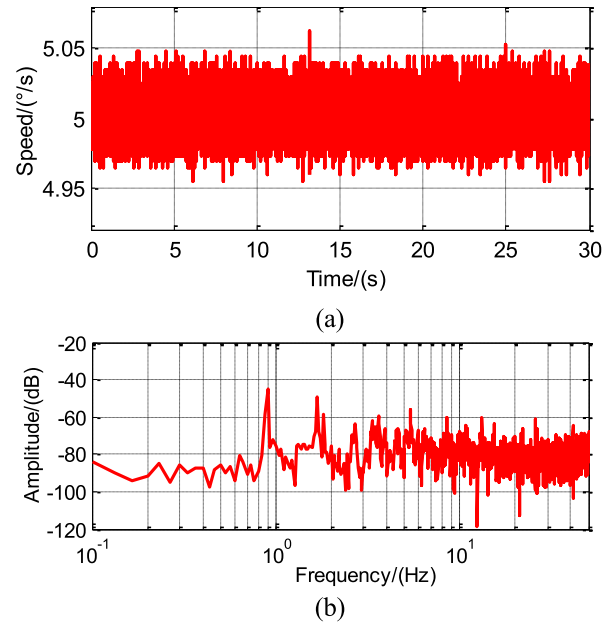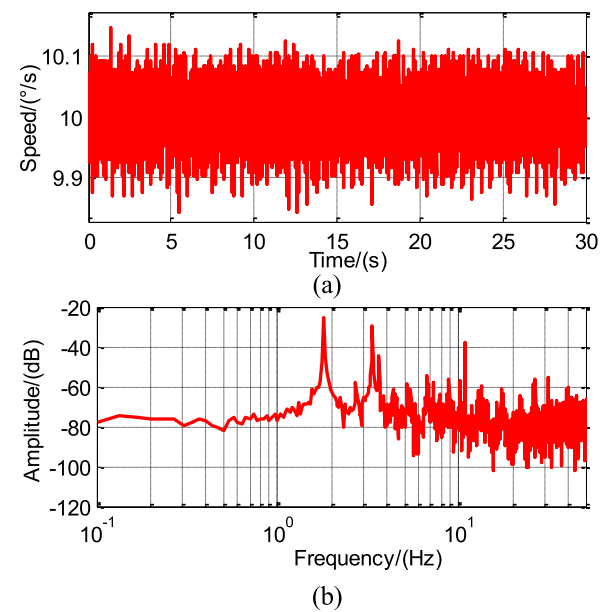
the PI and proposed controllers at 5° s⁻¹, respectively. The SRF is reduced from 4% to 1.8% for the MPC–ILC control. After calculation, the frequencies of the first, second, and sixth harmonics corresponding to 5° s⁻¹ are 0.903, 1.806, and 5.42 Hz, respectively. Figs. 7(b) and 8(b) present the Fourier analysis results of the corresponding speed signals, and the frequencies of the first, second, and sixth harmonics are 0.909, 1.81, and 5.43 Hz, respectively. The experimental results are almost identical to the calculated results. As can be seen, the amplitudes of the first, second, and sixth

**FIGURE 10.** Experimental results of the MPC–ILC control at 10° s$^{-1}$: (a) speed response and (b) frequency spectrum.

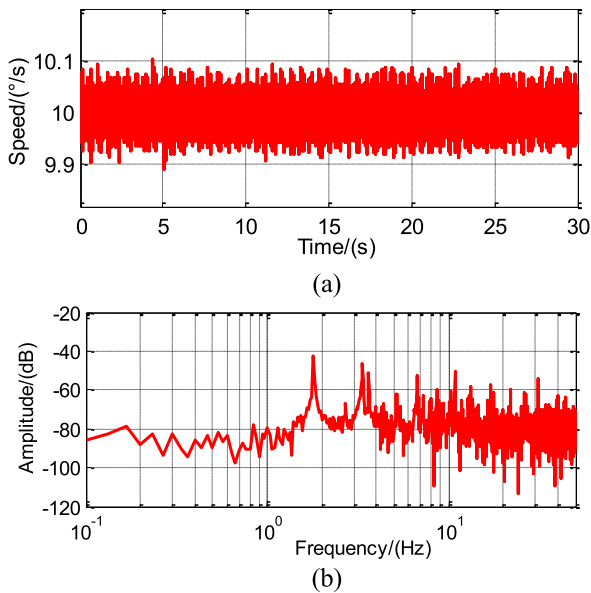harmonics are reduced from $-22.7$, $-31.1$, and $-36.5$ dB to $-44.9$, $-49.3$, and $-55.9$ dB, respectively. Figs. 9 and 10 are arranged in the same sequence for operating conditions at $10°$ s$^{-1}$. In these cases, the corresponding SRF is suppressed from 3.6% to 1.9%. The amplitudes of the first, second, and sixth harmonics are reduced from $-25.4$, $-29.6$, and $-38.1$ dB to $-42.5$, $-46.3$, and $-50.4$ dB, respectively. The experimental results show that the proposed control strategy can reduce the speed fluctuation to some extent and improve the stability of the servo system.

## VII. CONCLUSION

To minimize the torque ripple and enhance the performance of the PMSM drive systems, this paper proposed the combination of an MPC with an angle-based ILC. The proposed control scheme increases the speed response time and effectively suppresses the periodic velocity pulsation. This method is easy to implement on an integrated DSP-FPGA-based PMSM platform. The simulation and experimental results indicate that the proposed scheme can minimize the speed ripple effectively and further improve control performance.

## REFERENCES

[1] T. M. Jahns and W. L. Soong, "Pulsating torque minimization techniques for permanent magnet AC motor drives—A review," *IEEE Trans. Ind. Electron.*, vol. 43, no. 2, pp. 321–330, Apr. 1996.

[2] B. H. Lam, S. K. Panda, and J. X. Xu, "Reduction of periodic speed ripples in PM synchronous motors using iterative learning control," in *Proc. 26th Annu. Conf. IEEE Ind. Electron. Soc.*, Oct. 2000, pp. 1406–1411.

[3] W. Qian, S. K. Panda, and J. X. Xu, "Torque ripple minimization in PM synchronous motors using iterative learning control," *IEEE Trans. Power Electron.*, vol. 19, no. 2, pp. 272–279, Mar. 2004.

[4] H. Hu, J. Zhu, and Y. Guo, "Model predictive control of permanent magnet synchronous machine with reduced torque ripple," in *Proc. IEEE Int. Conf. Power Electron. Drive Syst.*, Oct. 2013, pp. 1478–1482.

[5] R. Myeroff, G. Mertlich, and J. Gross, "Torque ripple minimization in PM synchronous motors–an iterative learning control approach," *IEEE Trans. Power Electron.*, vol. 19, no. 2, pp. 272–279, Mar. 2004.

[6] K.-C. Kim, "A novel method for minimization of cogging torque and torque ripple for interior permanent magnet synchronous motor," *IEEE Trans. Magn.*, vol. 50, no. 2, pp. 793–796, Feb. 2014.

[7] W. Fei and P. C.-K. Luk, "Torque ripple reduction of a direct-drive permanent-magnet synchronous machine by material-efficient axial pole pairing," *IEEE Trans. Ind. Electron.*, vol. 59, no. 6, pp. 2601–2611, Jun. 2012.

[8] V. Petrović, R. Ortega, A. Stanković, and G. Tadmor, "Design and implementation of an adaptive controller for torque ripple minimization in PM synchronous motors," *IEEE Trans. Power Electron.*, vol. 15, no. 5, pp. 871–880, Sep. 2000.

[9] C. Lai, G. Feng, K. L. V. Iyer, K. Mukherjee, and N. C. Kar, "Genetic algorithm-based current optimization for torque ripple reduction of interior PMSMs," *IEEE Trans Ind Appl*, vol. 53, no. 5, pp. 4493–4503, Sep./Oct. 2017.

[10] T. Türker, U. Buyukkeles, and A. F. Bakan, "A robust predictive current controller for PMSM drives," *IEEE Trans. Ind. Electron.*, vol. 63, no. 6, pp. 3906–3914, Jun. 2016.

[11] A. Mora, A. Orellana, J. Juliet, and R. Cárdenas, "Model predictive torque control for torque ripple compensation in variable-speed PMSMs," *IEEE Trans. Ind. Electron.*, vol. 63, no. 7, pp. 4584–4592, Jul. 2016.

[12] Z. Ma, S. Saeidi, and R. Kennel, "FPGA implementation of model predictive control with constant switching frequency for PMSM drives," *IEEE Trans. Ind. Inform.*, vol. 10, no. 4, pp. 2055–2063, Nov. 2014.

[13] S. Wang, C. Xia, X. Gu, and W. Chen, "A novel FCS-model predictive control algorithm with duty cycle optimization for surface-mounted PMSM," in *Proc. 7th IET Int. Conf. Power Electron., Mach. Drives*, Apr. 2014, pp. 1–6.

[14] Y. Zhang and S. Gao, "Simultaneous optimization of voltage vector and duty cycle in model predictive torque control of PMSM drives," in *Proc. 17th Int. Conf. Elect. Mach. Syst. (ICEMS)*, Oct. 2014, pp. 3338–3344.

[15] H. Liu and S. Li, "Speed control for PMSM servo system using predictive functional control and extended state observer," *IEEE Trans. Ind. Electron.*, vol. 59, no. 2, pp. 1171–1183, Feb. 2012.

[16] X. Liu, C. Zhang, K. Li, and Q. Zhang, "Robust current control-based generalized predictive control with sliding mode disturbance compensation for PMSM drives," *ISA Trans.*, vol. 71, no. 2, pp. 542–552, Nov. 2017.

[17] R. Errouissi, A. Al-Durra, S. M. Muyeen, and S. Leng, "Continuous-time model predictive control of a permanent magnet synchronous motor drive with disturbance decoupling," *IET Electric Power Appl.*, vol. 11, no. 5, pp. 697–706, May 2017.

[18] R. Errouissi, M. Ouhrouche, and W. H. Chen, "Robust nonlinear generalized predictive control of a permanent magnet synchronous motor with an anti-windup compensator," in *Proc. IEEE Int. Symp. Ind. Electron.*, Nov. 2010, pp. 3184–3189.

[19] J. Liu, H. Li, and Y. Deng, "Torque ripple minimization of PMSM based on robust ILC via adaptive sliding mode control," *IEEE Trans. Power Electron.*, vol. 33, no. 4, pp. 3655–3671, Apr. 2018.

[20] S. Chai, L. Wang, and E. Rogers, "A cascade MPC control structure for a PMSM with speed ripple minimization," *IEEE Trans. Ind. Electron.*, vol. 60, no. 8, pp. 2978–2987, Aug. 2012.

[21] C. Studer, A. Keyhani, T. Sebastian, and S. K. Murthy, "Study of cogging torque in permanent magnet machines," in *Proc. IEEE Ind. Appl. Conf. 32nd IAS Annu. Meeting*, vol. 1, Oct. 1997, pp. 42–49.

[22] Z. Bien and JX. Xu, *Iterative Learning Control: Analysis, Design, Integration and Applications*. New York, NY, USA: Springer, 1998.

[23] B. H. Lam, S. K. Panda, and J. X. Xu, "Torque ripple minimization in PM synchronous motors an iterative learning control approach," in *Proc. IEEE Int. Conf. Power Electron. Drive Syst.*, vol. 19, no. 2, Jul. 1999, pp. 27–29.

[24] S. K. Sahoo, S. K. Panda, and J. X. Xu, "Application of spatial iterative learning control for direct torque control of switched reluctance motor drive," in *Proc. IEEE Power Eng. Soc. General Meeting*, Tampa, FL, USA, Jun. 2007, pp. 1–7.

[25] Y. Yuan, P. Auger, L. Loron, P. Debrailly, and M. Hubert, "Design of a lying sensor for permanent magnet synchronous machine torque ripple reduction using the iterative learning control technique," in *Proc. IEEE Int. Conf. Power Electron. Drive Syst.*, Dec. 2011, pp. 1–6.

[26] L. Zhu, S. Z. Jiang, Z. Q. Zhu, and C. C. Chan, "Analytical methods for minimizing cogging torque in permanent-magnet machines," *IEEE Trans. Magn.*, vol. 45, no. 4, pp. 2023–2031, Apr. 2009.

[27] L. Dosiek and P. Pillay, "Cogging torque reduction in permanent magnet machines," *IEEE Trans. Ind. Appl.*, vol. 43, no. 6, pp. 1565–1571, Nov. 2007.

[28] S. Boming, "On iterative learning control," Ph.D. dissertation, National Univ. Singapore, Singapore, 1996.

**QIANG FEI** was born in Shandong, China, in 1993. He received the B.E. degree from Weifang University, in 2015. He is currently pursuing the Ph.D. degree with the University of Chinese Academy of Sciences and the Changchun Institute of Optics, Fine Mechanics and Physics, Chinese Academy of Sciences, China.

His research interests include AC motor drive and control design, model predictive control, and digital control using DSP.
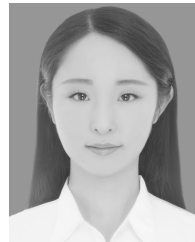
**YONGTING DENG** was born in Shandong, China, in 1987. He received the B.E. degree from the China University of Petroleum, China, and the M.S. and Ph.D. degrees from the Changchun Institute of Optics, Fine Mechanics and Physics, Chinese Academy of Sciences, China, in 2015.

He is currently an Associate Professor with the Changchun Institute of Optics, Fine Mechanics and Physics, Chinese Academy of Sciences. His research interests include controller design for ac motor drives and linear motor drives, intelligent control, and digital control using the DSP and FPGA implementations.

**HONGWEN LI** was born in Sichuan, China, in 1970. He received the M.S. degree from the Jinlin University of Technology, China, in 1996, and the Ph.D. degree from Jinlin University, China, in 2007.

From 1996 to 2002, he was an Associate Professor with the Jinlin University of Technology. Since 2002, he has been with the Changchun Institute of Optics, Fine Mechanics, and Physics, Chinese Academy of Sciences, China, where he is currently a Professor with the Department of Optical-Electronic Detection. He has authored/co-authored more than 50 publications in his main areas of research, which are optical-electric sensor technologies, switching-mode power supply techniques, electric machines and drives, and high-precision machine control techniques.

**JING LIU** was born in Liaoning, China, in 1991. She received the B.E. degree from the Nanjing University of Aeronautics and Astronautics, China, in 2013, and the M.S. and Ph.D. degrees from the Changchun Institute of Optics, Fine Mechanics and Physics, Chinese Academy of Sciences, China, in 2017, where she is currently a Staff Member.

Her research interests include electric machines and drives and high-precision machine control techniques.

**MENG SHAO** was born in Jilin, China, in 1992. He received the B.E. degree from Northeastern University, China, in 2015. He is currently pursuing the Ph.D. degree with the University of Chinese Academy of Sciences and the Changchun Institute of Optics, Fine Mechanics and Physics, Chinese Academy of Sciences, China.

His research interests include electric machines and drives, high-precision machine control techniques, and digital control using the DSP and FPGA implementations.

● ● ●